

A NURBS-based interface-enriched generalized finite element method for problems with complex discontinuous gradient fields

Masoud Safdari^{1,*}, Ahmad R. Najafi², Nancy R. Sottos³ and Philippe H. Geubelle¹

¹*Department of Aerospace Engineering, University of Illinois, Urbana, IL 61801, USA*

²*Department of Mechanical Science and Engineering, University of Illinois, Urbana, IL 61801, USA*

³*Department of Materials Science and Engineering, University of Illinois, Urbana, IL 61801, USA*

SUMMARY

A non-uniform rational B-splines (NURBS)-based interface-enriched generalized finite element method is introduced to solve problems with complex discontinuous gradient fields observed in the structural and thermal analysis of the heterogeneous materials. The presented method utilizes generalized degrees of freedom and enrichment functions based on NURBS to capture the solution with non-conforming meshes. A consistent method for the generation and application of the NURBS-based enrichment functions is introduced. These enrichment functions offer various advantages including simplicity of the integration, possibility of different modes of local solution refinement, and ease of implementation. In addition, we show that these functions well capture weak discontinuities associated with highly curved material interfaces. The convergence, accuracy, and stability of the method in the solution of two-dimensional elasto-static problems are compared with the standard finite element scheme, showing improved accuracy. Finally, the performance of the method for solving problems with complex internal geometry is highlighted through a numerical example. Copyright © 2015 John Wiley & Sons, Ltd.

Received 28 February 2014; Revised 7 November 2014; Accepted 11 November 2014

KEY WORDS: NURBS; GFEM; weak discontinuity

1. INTRODUCTION

A large number of boundary value problems in continuum mechanics and other engineering disciplines involve non-smooth solution fields that are weakly discontinuous (C^0 -continuous). For instance, a jump in the gradient of the displacement or temperature field in heterogeneous materials is expected along the material or phase interfaces. Such problems are generally described by a governing differential equation with discontinuous coefficients. The finite element analysis (FEA) is one of the standard numerical methods which is highly suited for the approximation of the solution to smooth problems. In order to utilize FEA for problems with gradient discontinuities, a mesh needs to be generated in which the edges/surfaces of the elements conform to these discontinuities to utilize the inherent C^0 -continuity properties of the elements in these places. For a problem with complex-shaped discontinuities, such mesh generation step is very complicated and tedious. Similarly, the same approach requires cumbersome re-meshing steps for problems with evolving discontinuities.

Over the past 20 years, more generalized forms of FEA have been developed including the extended FEM (XFEM) and generalized FEM (GFEM) [1–4]. These methods are mostly developed to reduce expensive mesh generation/evolution steps and to enable the FEA to handle discontinuous

*Correspondence to: Masoud Safdari, Department of Aerospace Engineering, University of Illinois, 104 S. Wright St., Urbana, IL 61801, USA.

†E-mail: msafdari@illinois.edu

problems with non-conforming meshes. In a generalized framework, to account for solution discontinuities, a number of new degrees of freedom (dofs) are added to the nodes of the elements existing in the neighborhood of these discontinuities, and the finite element approximation space is locally enhanced with *a priori* known enrichment functions. Through these enrichment functions and extra dofs, discontinuities not affordable by standard polynomial shape functions can be captured. The augmentation of the polynomial space of the standard FEA with enrichment functions is usually realized through the partition-of-unity concept [1, 5]. For instance, to account for the presence of strong discontinuities associated with a crack, the approximation space has been enhanced with discontinuous enrichment functions [6, 7]. These basis functions added to the approximation space should be linearly independent to guarantee an invertible system of equations. Therefore, special treatments are sometimes needed to generate and apply these enrichment functions in order to guarantee the convergence [8, 9]. Other difficulties for GFEM methods are the complexity of their implementation [10] and the large number of additional dofs, which they may introduce.

GFEM approaches have been successfully used in problems with weak discontinuities, and many research efforts are devoted to the identification of the new enrichment functions for this purpose [11–18]. Recently, Soghrati *et al.* [10] have introduced a novel method based on the framework of GFEM to solve these types of problems. In this method, named interface-enriched GFEM (or IGFEM), additional dofs are introduced in the solution along the intersections of the material interfaces with the edges/faces of the non-conforming mesh. Placing enrichment dofs along the intersection points eliminates some of the previously mentioned implementation issues associated with the GFEM methods [8, 9]. Additionally, the enrichment functions utilized by this method require no special treatment. These functions are constructed from the first-order Lagrangian polynomials, and they best capture linear weak discontinuities. With such first-order approximation to the solution field around weak discontinuities, it was shown in [10] that a precise solution can be captured for problems with simple interfaces. In order to consider more complex interfaces or to capture a higher accuracy solution, the method utilizes more dense non-conforming meshes.

In the current study, we build on the IGFEM by introducing more flexible enrichment functions. Non-uniform rational B-splines (NURBS) [19] are employed as a basis to represent enrichment functions in the framework of IGFEM; therefore, the current approach is referred to hereafter as NURBS-based IGFEM (NIGFEM). This approach utilizes some of the concepts of the isogeometric analysis (IGA) [20], which provides superior advantages for solving problems with complex domains and a more accurate solution under an optimal rate of convergence [20, 21]. These promising features have increased the popularity of the IGA in many fields such as structural mechanics [20], solid-fluid interactions [22], structural vibration [23], and even for problems with higher-order governing differential equations [24]. Moreover, IGA has been recently applied to the problems with strong discontinuities [25, 26].

The current work integrates some of the IGA concepts into the IGFEM in a two-dimensional (2D) setting. Related approaches to this work can be found in [27–29], which use the standard IGA to describe a solution field piecewise defined by the trimmed NURBS. Such approaches are very interesting when trimmed NURBS geometries (usually provided with computer-aided design (CAD)) are defined within a unique parametric space. Trimmed NURBS-based IGA can find solutions in domains with any number of vacant cavities. However, it does not allow for heterogeneities. In practice, such constraints restrict the application of the trimmed NURBS analysis to simple CAD models constructed with boolean operations. For more general domains, like the microstructure of the heterogeneous materials, providing a trimmed NURBS representation is not practical. Another difficulty arises during the numerical integration of the complex parametric spaces defined by the trimmed NURBS geometries. NIGFEM, unlike IGA and its trimmed NURBS extension, does not restrict the solution field to a specific unique approximation and parametric space. Moreover, the method offers a straightforward numerical integration procedure and provides most of the advantages of the GFEM/XFEM.

The rest of this paper is organized as follows. In Section 2, the NIGFEM formulation for linearly elastic boundary value problems is provided. The implementation steps of the NIGFEM including the construction of the NURBS enrichment functions and the proposed numerical integration are discussed in this section as well. In Section 3, the robustness, effectiveness, and convergence of

NIGFEM are compared with those of the regular FEM and IGFEM. To highlight the capabilities of the presented method, an application problem solved by NIGFEM is discussed in Section 4. Section 5 summarizes the important features of the method and provides concluding remarks.

2. NIGFEM: FORMULATION AND IMPLEMENTATION

2.1. Basic formulation

Let $\mathcal{S}^h \subset \mathbf{S}$ and $\mathcal{V}^h \subset \mathbf{V}$ denote the solution and weight spaces, respectively. The Galerkin weak statement to the elasto-static problems involves finding $\mathbf{u}^h \in \mathcal{S}^h$ such that

$$a(\mathbf{w}^h, \mathbf{u}^h) = L(\mathbf{w}^h) \quad \forall \mathbf{w}^h \in \mathcal{V}^h, \quad (1)$$

in which the bilinear term $a(\mathbf{w}^h, \mathbf{u}^h)$ and linear term $L(\mathbf{w}^h)$ are defined by

$$a(\mathbf{w}^h, \mathbf{u}^h) = \int_{\Omega} \nabla \mathbf{w}^h : \boldsymbol{\sigma} d\Omega, \quad (2)$$

$$L(\mathbf{w}^h) = \int_{\Omega} \mathbf{w}^h \cdot \mathbf{F} d\Omega + \int_{\Gamma_T} \mathbf{w}^h \cdot \mathbf{T} d\Gamma, \quad (3)$$

where \mathbf{w}^h is the weight function, $\boldsymbol{\sigma}$ denotes the stress tensor, Ω is the domain, Γ_T is the portion of the boundary under traction, and \mathbf{F} and \mathbf{T} are the body force and applied tractions, respectively. By discretizing the domain into m finite elements ($\Omega \cong \Omega^h = \bigcup_{i=1}^m \bar{\Omega}_i$), one can use the weak statement (1) directly to find a finite element approximation to the solution field as

$$\mathbf{u}^h(\mathbf{x}) = \sum_{i=1}^n N_i(\mathbf{x}) \mathbf{u}_i, \quad (4)$$

where $N_i(\mathbf{x})$ is a set of basis functions taken from Lagrangian space, n is the number of nodes, and \mathbf{u}_i denote the displacement dofs. However, this approximation to the solution field requires a conforming mesh that maintains C^0 -continuity along material interfaces. To adopt a non-conforming mesh, the solution field is augmented by enrichment dofs $\boldsymbol{\alpha}_j$ and enrichment functions $\Psi_j(\mathbf{x})$ as

$$\mathbf{u}^h(\mathbf{x}) = \sum_{i=1}^n N_i(\mathbf{x}) \mathbf{u}_i + \sum_{j=1}^{n_{en}} \Psi_j(\mathbf{x}) \boldsymbol{\alpha}_j, \quad (5)$$

in which n_{en} is the number of enrichments. It should be emphasized that, in the current formulation, there is no restriction for the type of basis functions $N_i(\mathbf{x})$ utilized for the standard part of the finite element solution. In this study, standard Lagrangian shape functions are used for $N_i(\mathbf{x})$, and NURBS are used only to construct the enrichment functions $\Psi_j(\mathbf{x})$. Another notable difference between NIGFEM and more regular GFEM/XFEM is the fact that, in NIGFEM, the additional dofs $\boldsymbol{\alpha}_j$'s are introduced along the interface instead of being added to the nodes of the non-conforming mesh. In order to capture a curvilinear interface, we construct enrichment functions $\Psi_j(\mathbf{x})$ using NURBS basis functions. The adopted number of NURBS basis functions (n_{en}) depends on the order of the NURBS curve representing the interface, its level of complexity, and the level of discretization of the non-conforming mesh. Further details about the construction of the NURBS enrichment functions are provided in the next section.

2.2. Enrichment functions

Let us consider a domain discretized with standard bilinear quadrilateral elements and a material interface with complex geometry represented by a univariate NURBS curve:

$$C(w) = \sum_{k=1}^n \bar{N}_k(w) \mathbf{P}_k, \tag{6}$$

where n is the number of control points of $C(w)$, \bar{N}_k 's are the NURBS basis function, and \mathbf{P}_k 's are the control points of $C(w)$. It should be noted that the parametric coordinate $w \in \mathcal{W}$ is chosen in the interval of the knot vectors defined by

$$\mathcal{W} = [w_1, \dots, w_{n+p+1}], \tag{7}$$

where w_i are the knot values and p is the order of the NURBS basis for $C(w)$. To perform an IGA on a heterogeneous/multiphase domain, like the one shown in Figure 1a, one has to subdivide it into a number of NURBS patches that conform to the material interface, as suggested by Figure 1b. These NURBS patches share their edges with the interface; thus, they naturally satisfy C^0 -continuity requirements along the material interface. To avoid the need for these conforming NURBS patches, the NIGFEM allows for non-conforming meshes, as shown in Figure 1a, and only requires the position of the intersection points between the element edges and the material interface. These intersection points can be found simply with point-inversion methods. Fast and reliable algorithms have been proposed for this purpose [30]. It is worth mentioning that, by increasing the complexity of the material interface(s), the computational cost of finding the intersection points for the NIGFEM is only a fraction of that of creating conforming NURBS patches needed for the IGA.

Once the intersection points are identified, the enrichment functions can be constructed. For this purpose, we refine the interface (with knot vector \mathcal{W}) at knot values associated with the intersection points. The multiplicity of the knot values is dictated by the order p of $C(w)$. Let us represent the refined interface curve by $C'(w)$. After the knot refinement, the mathematical continuity of the basis functions of $C'(w)$ with support over these intersection points is reduced to C^0 . However, the geometric continuity of $C'(w)$ remains untouched, and it represents $C(w)$ with a number of additional control points ($n' > n$). Up to this point, each intersecting element has a subsection of the interface, and each subsection only relies on a subset of the control points with support on that element. In the next step, for each intersecting element, we utilize these subsets of the control points and the topological information of that element to construct NURBS patches for the split subdomains. In the current study, for simplicity purposes, the order of $C(w)$ is selected to be $p = 2$;

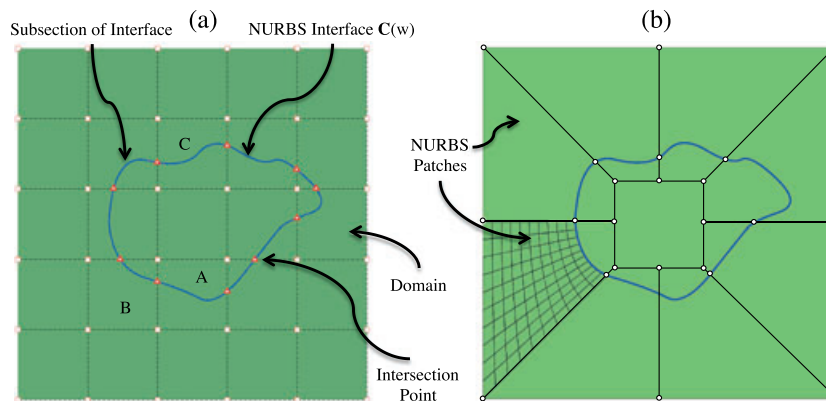


Figure 1. Illustration of the contrast between (a) the proposed NIGFEM approach and (b) the traditional IGA based on conforming NURBS patches.

therefore, the order for each split subdomain is selected to be $p_u = 2$ along the curvilinear interface direction (u) and $p_v = 1$ in the normal direction (v). It is worth mentioning that, for higher-order NURBS curves, the same approach is applicable.

In a 2D analysis, two different situations are possible when an interface intersects a quadrilateral element. It may intersect with two opposite edges of the element and divide it into two curvilinear quadrilateral regions, like elements A and C in Figure 1a, or the interface may divide an element into a curvilinear triangle and a curvilinear pentagon, as is the case for the element B in Figure 1a. In this work, we do not allow for the more complex case of which a high-curvature interface intersects an element edge more than once. In this case, it is always possible to further refine the mesh until it falls into one of the situations described earlier.

To better understand the process, let us show how the enrichment functions are constructed for the element C shown in Figure 1a. The material interface cuts this element into two curvilinear quadrilateral split subdomains S_1 and S_2 . To generate enrichment functions for this element, we first need to construct 2D NURBS patches of these split subdomains. For this purpose, we select all control points of $C'(w)$ that are associated with the basis functions with support over C. For this element, four control points of $C'(w)$ reside in the element space labeled by $P_{1,j}$ ($j = 1 \dots 4$), shown in Figure 2a. We also take four dummy control points along the edge of S_1 parallel to the interface subsection, $P_{2,j}$ ($j = 1 \dots 4$). The initial and final control points $P_{2,j}$ are the two vertices of the element C, and those in-between are selected uniformly along the edge that connects these vertices. We call these control points dummy because no dof is associated with them, and they are just used to construct NURBS patches. To construct the NURBS patch for S_1 , a knot vector along each of the parametric directions is also needed. For the direction parallel to the interface (u), we simply select the knot span \mathcal{U}_c , corresponding to the subsection of $C'(w)$ that resides in the element C. For the normal direction (v), the simplest choice is a linearly interpolating NURBS basis with the associated knot vector $\mathcal{V}_c = [0, 0, 1, 1]$. With the selected coefficients $P_{i,j}$ ($i = 1, 2, j = 1 \dots 4$), and the knot vectors, \mathcal{U}_c and \mathcal{V}_c , we can create a 2D NURBS patch for S_1 . We take the same approach to construct a 2D NURBS patch for S_2 using $P_{i,j}$ ($i = 1, 3, j = 1 \dots 4$) and the same knot vectors \mathcal{U}_c and \mathcal{V}_c . Let us label the basis functions associated to each subdomain by $\bar{N}_{i,j}^{S_1}$ and $\bar{N}_{i,j}^{S_2}$ ($i = 1, 2, j = 1 \dots 4$). Element C in this example has four NURBS enrichment functions $\Psi_j(\mathbf{x})$ corresponding to each control point along the material interface. These enrichment functions are simply constructed from $\bar{N}_{i,j}^{S_1}$ and $\bar{N}_{i,j}^{S_2}$ through

$$\Psi_j(\mathbf{x}) = \begin{cases} \bar{N}_{1,j}^{S_1}(\mathbf{x}) & \mathbf{x} \in S_1 \\ \bar{N}_{1,j}^{S_2}(\mathbf{x}) & \mathbf{x} \in S_2 \end{cases} \quad j = 1 \dots 4. \tag{8}$$

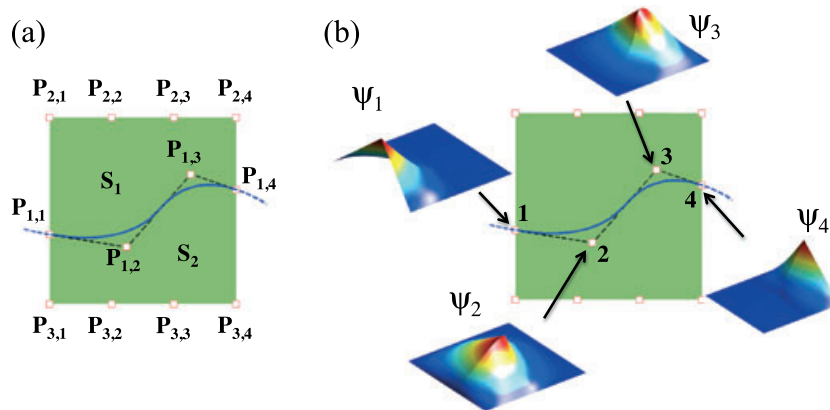


Figure 2. (a) Construction of element subdomains. (b) NURBS-based enrichment functions associated with the four control points defining a curved interface.

The same approach is taken to construct enrichment functions for the elements that are split into a curvilinear triangle and a curvilinear pentagon, for example, the element B shown in Figure 1a. However, in order to recreate the sharp corners, we superpose a number of dummy control points on top of each other. For example, for a quadratic NURBS curve $C(w)$, at least two superposed dummy control points are used to recreate the sharp corner in the NURBS patches. Figure 3 depicts these cases and the suggested strategies to construct the NURBS patches B_1 and B_2 . In each case, $P_{1,i}$ and $P_{2,i}$ are two iso-curves of the NURBS patch corresponding to $v = 0$ and 1, respectively.

The variation of the enrichment functions for the element C is depicted in Figure 2b. As apparent there, these functions accurately regenerate the material interface geometry in this element, and they only take values along the interface and rapidly vanish away from the interface to the corners. Furthermore, these functions are naturally C^0 -continuous along the interface. Thus, they can reproduce a discontinuous gradient across the material interfaces by augmenting the approximation space. These properties make them a natural selection for the enrichment purpose, $\Psi_j(\mathbf{x})$, in Equation (5).

2.3. Integration

In the NIGFEM framework, the construction of NURBS patches serves two purposes. First, the enrichment functions are constructed from the basis functions of these patches, as discussed in the pervious section. Second, these patches are directly used for the purpose of the numerical integration of the weak form. In fact, each NURBS patch is generated by mapping a simple rectangular parametric space to a complex physical space. Thus, to perform a numerical integration over the NURBS patches, one can map this parametric space directly into master element space and then utilize a high-order Gauss quadrature scheme. This approach is referred to hereafter as *patch-wise mapping* (PWM). However, another approach is to map each non-vanishing knot-span of the parametric space of each patch into the master element space and then employ a less expensive Gauss quadrature scheme. The latter approach is referred to hereafter as *span-wise mapping* (SWM). Both of these approaches have been suggested previously in [16, 27, 28]. As depicted in Figure 3, for each patch with two non-vanishing knot spans in the parametric direction u and one knot span in

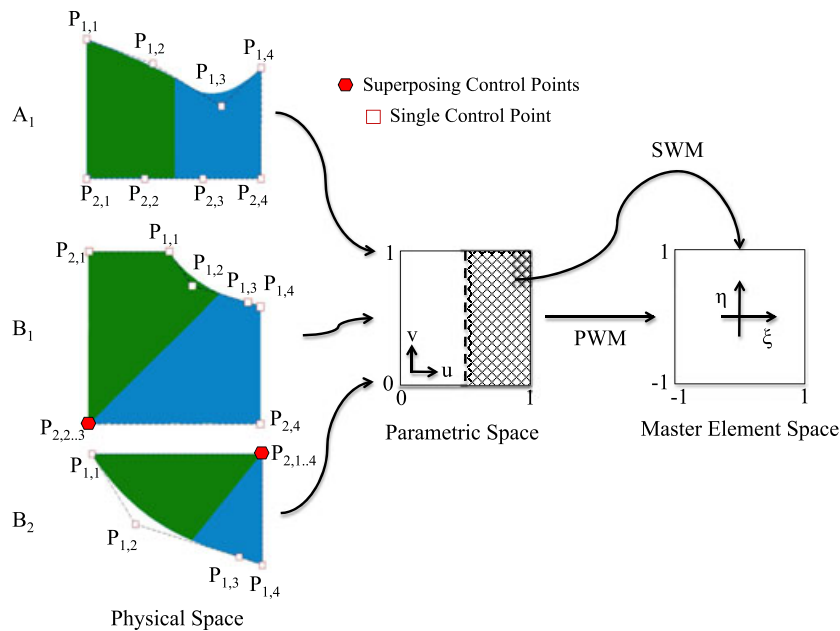


Figure 3. Possible geometric cases arising from the intersection of an interface with a quadrilateral element.

the parametric direction v , PWM maps the whole parametric space into the master element space, while SWM maps each non-vanishing knot span into the master element space separately.

Aside from the mapping strategy, it should be noted that NURBS are in general rational B-Spline functions which cannot be integrated exactly by Gauss quadrature. In fact, the numerical integration of NURBS functions is still an active area of research [16, 27, 31, 32]. Furthermore, the shape of a NURBS patch also adds complexity to the numerical integration [33, 34]. For instance, at the superposing control points used to construct the subdomains B_1 and B_2 shown in Figure 3, the mapping between the physical space and the parametric NURBS space is singular. Therefore, during the numerical integration of the weak form for such elements, the Jacobian is singular at these points. Singular functions are also observed in other GFEM/XFEM schemes [35], and their numerical integration is also an active area of research [36, 37].

Figure 4 compares the accuracy of the PWM and SWM schemes in the numerical integration over the NURBS patch Ω_1 for $r \in [0, \sqrt{2}l]$. As shown in Figure 4a, for $r/l < 1$, the patch Ω_1 is a curvilinear pentagon, while for $r/l > 1$, the patch Ω_1 changes to a curvilinear triangle (Figure 4b). Figure 4c and d presents the accuracy of both schemes for the numerical evaluation of the area of Ω_1 . For the calculation of the area, the integrand is a constant (unity) function, and the Jacobian determinant can be considered to be at least a quadratic function. Therefore, a 2×2 scheme is deemed to be enough. By comparing 2×2 schemes, we observe that there is a jump in the accuracy of the quadrature computed by both schemes at $r/l = 1$. This jump corresponds to the aforementioned change in the morphology of the patch Ω_1 from the curvilinear pentagon (Figure 4a) to the curvilinear triangle (Figure 4b). The singularity of the Jacobian matrix at the superposing control points of Ω_1 also reduces the accuracy of the numerical integration. It is observed that, under the same conditions, the SWM scheme is more accurate compared with the PWM scheme.

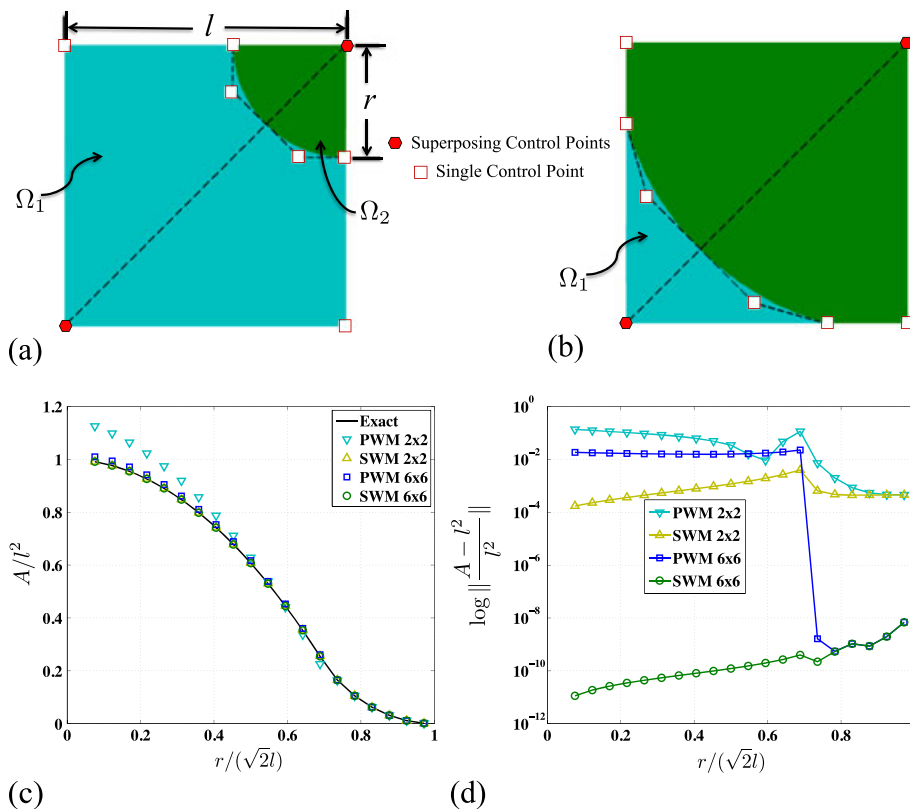


Figure 4. (a) Integration domain defined by NURBS patches Ω_1 for $r \in [0, l]$, and (b) $r \in [l, \sqrt{2}l]$. (c, d) Comparison between the PWM and SWM schemes in the numerical integration of the area A of the patch Ω_1 .

The detrimental effect of the superposing control points of a NURBS patch is also confirmed in [33, 34]. A closer look at Figure 4d reveals that for this problem, a 2×2 SWM scheme outperforms even a 6×6 PWM scheme over a large portion of the interval $r \in [0, \sqrt{2}l]$. These observations suggest that the SWM scheme is generally more efficient than the PWM scheme and is therefore adopted in the remainder of this study.

3. CONVERGENCE STUDY

Figure 5a shows the geometry and imposed boundary conditions of the problem selected to test the convergence and accuracy of NIGFEM. The problem domain consists of a circular inclusion Ω_1 embedded in a unit-size square $\Omega_1 \cup \Omega_2 = \Omega$, with the stiffness ratio $E_2/E_1 = 2$, and the Poisson's ratio $\nu_1 = \nu_2 = 0.3$, yielding a weakly continuous displacement field along the interface. Figure 5b shows a sample non-conforming mesh made of bilinear quadrilateral elements used in the NIGFEM analysis. The accuracy and convergence of NIGFEM are quantified with the aid of the following error measures:

$$\|\mathbf{u} - \mathbf{u}^h\|_{L_2(\Omega)} = \sqrt{\frac{\int_{\Omega} \|\mathbf{u} - \mathbf{u}^h\|^2 d\Omega}{\int_{\Omega} \|\mathbf{u}\|^2 d\Omega}}, \tag{9}$$

$$\|e\|_{\Omega} = \sqrt{\frac{\int_{\Omega} (\boldsymbol{\varepsilon} - \boldsymbol{\varepsilon}^h) : (\boldsymbol{\sigma} - \boldsymbol{\sigma}^h) d\Omega}{\int_{\Omega} \boldsymbol{\varepsilon} : \boldsymbol{\sigma} d\Omega}}, \tag{10}$$

where the reference displacement \mathbf{u} , strain $\boldsymbol{\varepsilon}$, and stress $\boldsymbol{\sigma}$ are determined using a very fine conforming finite element mesh of bilinear quadrilateral elements (mesh size $h \simeq 0.005$). For the purpose of comparison, the same problem is also solved by the IGFEM scheme [10] as well.

Figure 6a illustrates the rate of convergence of the NIGFEM, FEM, and IGFEM solutions in terms of the L_2 -norm with respect to the mesh size h . As apparent there, the NIGFEM provides a convergence rate almost identical to the FEM solution obtained with a conforming mesh, with a

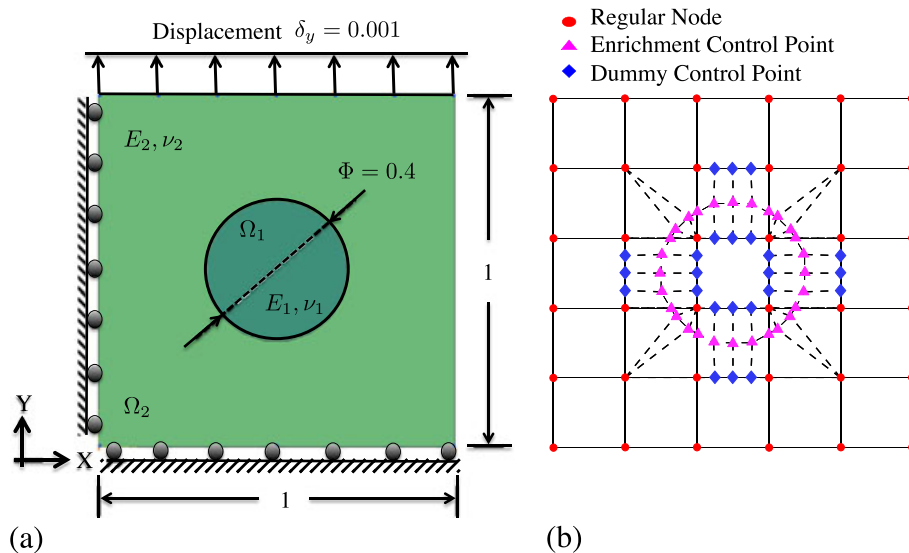


Figure 5. (a) Domain and boundary conditions of the convergence study problem. (b) A structured 5×5 rectilinear mesh composed of bilinear quadrilateral elements with mesh size $h = 0.2$ used in the NIGFEM and IGFEM analyses.

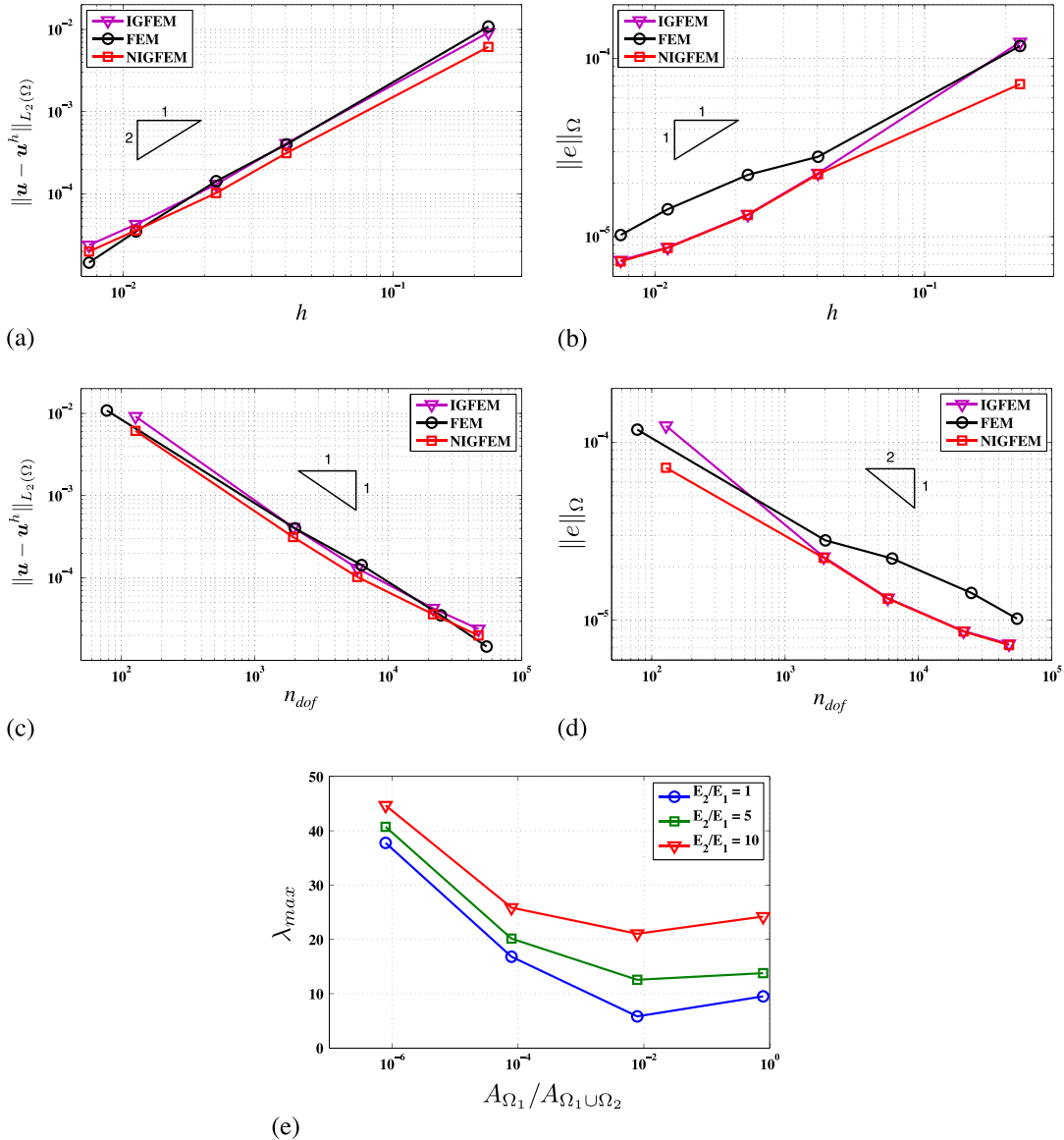


Figure 6. Comparison between the rate of convergence provided by the NIGFEM, IGFEM, and FEM with respect to mesh size h in terms of (a) L_2 -norm and (b) energy-norm and with respect to the number of degrees of freedom n_{dof} in terms of (c) L_2 -norm and (d) energy-norm. (e) Variation of the largest eigenvalue λ_{max} of the stiffness matrix for an enriched element with respect to the ratio between the areas of its NURBS patches and for three values of the stiffness ratio.

better accuracy. NIGFEM also provides a rate of convergence identical to the IGFEM but with better accuracy for the same non-conforming mesh. The improvement in precision associated with the NIGFEM is due to a more accurate representation of the geometry of the material interfaces and of the solution in the immediate vicinity of these interfaces. As expected, the rate of convergence of the NIGFEM is governed by that of the underlying finite element discretization, that is, bilinear quadrilateral elements in the present study. As presented in Figure 6b, a comparison between the energy norms shows that the NIGFEM also provides a better approximation for the gradient of the solution field compared with the FEM solution. With respect to the total number of dofs (including standard and enrichment dofs), n_{dof} , a comparison between these methods for the same error measures also shows similar trends for the NIGFEM and FEM, as shown in Figure 6c and d.

A closer look at Figure 6a and c reveals that, for coarse meshes, NIGFEM outperforms FEM and IGFEM. However, for the highly refined meshes, NIGFEM and IGFEM start to lose their optimality, mainly because of the formation of ill-conditioned enriched elements. In these elements, material interfaces pass very closely from one of the nodes of the non-conforming mesh and cut the element into two patches with a large difference in their area. To illustrate this point, Figure 6e depicts the variation of the largest eigenvalue λ_{max} of the stiffness matrix of the element shown in Figure 4a. As indicated there, it can be observed that, by increasing the ratio between the area of the patches Ω_1 and Ω_2 , λ_{max} increases substantially. Such enriched elements are numerically stiff, and their stiffness matrix is rank deficient. With an increase in the number of such elements, λ_{max} for the global stiffness matrix of the system also increases. Such linear system is more sensitive to the truncation errors, and the solution to such system is less accurate. With very fine meshes, the formation of such stiff enriched elements is more probable. The formation of these misbehaving enriched elements is also reported by other XFEM/GFEM studies [38, 39]. Another source for increasing λ_{max}

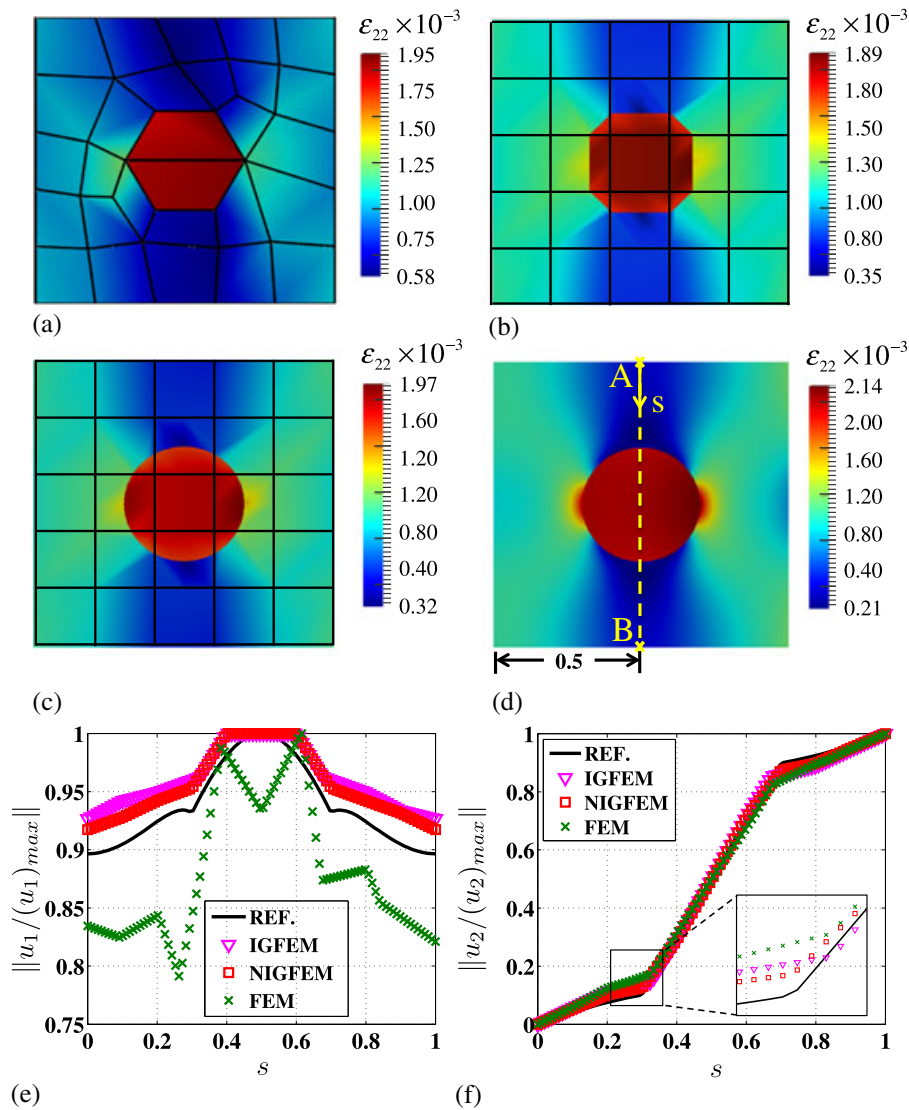


Figure 7. Distribution of the strain component ϵ_{22} for $E_2/E_1 = 10$ computed from (a) regular FEM ($h = 0.2$), (b) IGFEM solution ($h = 0.2$), (c) NIGFEM solution ($h = 0.2$), and (d) reference FEM ($h = 0.005$). The variation of normalized (e) u_1 and (f) u_2 displacements along line $A - B$. The inset compares the accuracy of all of the methods close to the material interface.

is the presence of superposing control points in the NURBS patches [33, 34]. However, increasing the order of the NURBS basis can enhance the behavior of these elements [33]. Another possible remedy is to pass the interface exactly through the node in such situations to avoid the formation of these elements in the first place.

To conclude this convergence study, we note that, over the range of coarse meshes and with complex material interfaces, NIGFEM performs better than regular FEM and IGFEM. To highlight the performance of the NIGFEM scheme over a coarse discretization, the distribution of the ε_{22} strain component captured by regular FEM, IGFEM, NIGFEM, and the reference (highly refined) FEM schemes are shown in Figure 7a–d, respectively. IGFEM and NIGFEM utilize a structured mesh of bilinear quadrilateral elements (shown in Figure 5b) enriched in the intersecting elements with linear Lagrangian and quadratic NURBS enrichment functions, respectively. The conventional FEM solution is captured by an unstructured conforming mesh of bilinear quadrilateral elements with approximately the same level of refinement ($h = 0.2$). As expected, in contrast with FEM and IGFEM, the NIGFEM preserves the exact geometry of the inclusion regardless of the mesh size utilized. In fact, the NIGFEM affords to recover weak discontinuities perfectly through a few added enrichment functions and dofs. A close examination reveals that the NIGFEM also provides a better approximation to the gradient of the solution field. As shown in Figure 7e and f, the variation of the displacement components u_1 and u_2 along the line $A - B$ also highlights the better accuracy of the NIGFEM.

It is known that a large mismatch between the material properties of a heterogeneous media introduces large gradient jumps in the solution field. The effect of the material mismatch ratio (E_2/E_1) on the solution provided by the NIGFEM method is depicted in Figure 8a and b, showing that the accuracy of the NIGFEM decreases with the increasing material mismatch, as also reported for the GFEM [40]. To explain this result, we refer to the study illustrated in Figure 6e, where we observed that λ_{max} increases with the stiffness mismatch E_2/E_1 . Therefore, a lower

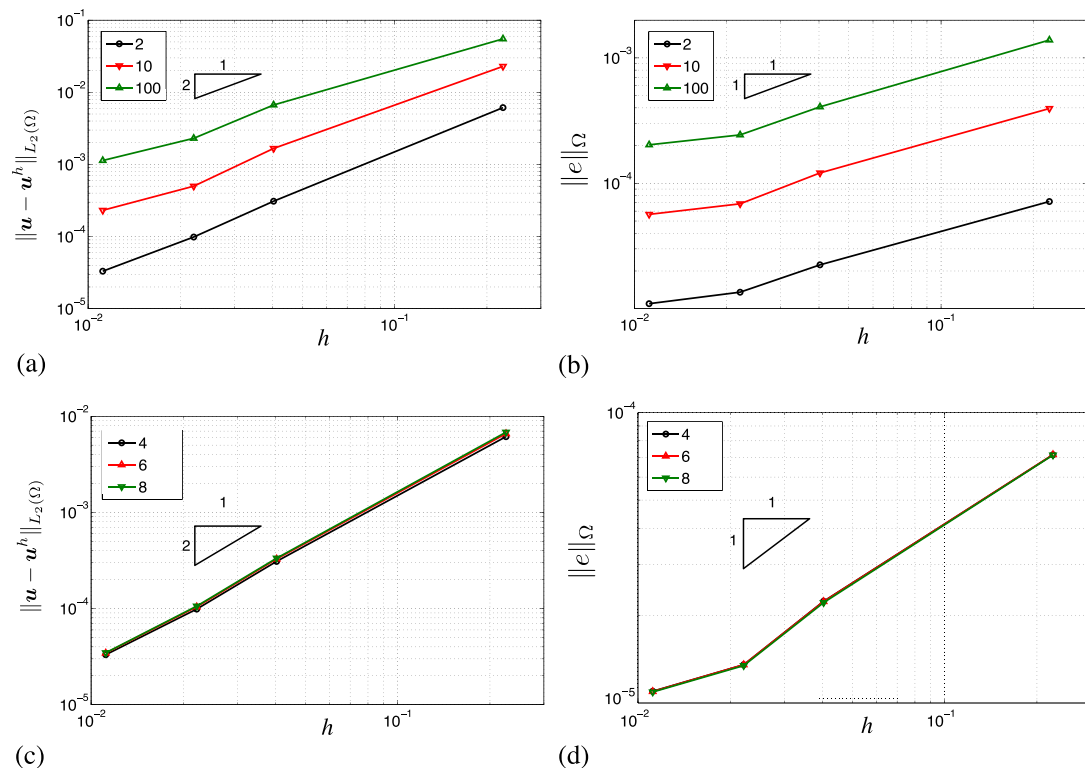


Figure 8. Effect of material mismatch (E_2/E_1) (top figures) and number of enrichment functions per element (bottom figures) on the convergence and accuracy of the NIGFEM solution. (a, c) L_2 -norm of the error; (b, d) energy norm.

quality solution is expected. As another degree of flexibility, NIGFEM allows for arbitrary number of enrichment functions for each enriched element. This feature enables the method to capture solutions for complex interfaces with coarse non-conforming meshes. As shown in Figure 8c and d, NIGFEM provides identical accuracy for the solution and its gradient by increasing the number of enrichment functions in each enriched element from four to six and eight. In this example with a quadratic NURBS interface geometry, four enrichment functions are enough to capture the right solution.

4. APPLICATION PROBLEM

To highlight the application of the presented method, the model plane stress problem shown in Figure 9a is solved with the NIGFEM scheme. Three complex shape inclusions Ω_2 , Ω_3 , and Ω_4 with properties E_2, ν_2 are embedded in a unit-size L-shaped matrix material (E_1, ν_1). The contrast between the properties is selected such that $E_2/E_1 = 10$ and $\nu_1 = \nu_2 = 0.3$. A uniform displacement $\delta_x = 0.001$ is applied to the lower boundary of the domain while the upper-left boundary is kept fixed. A relatively coarse structured mesh made of bilinear quadrilateral elements ($h = 0.02$) with a total of approximately 5000 dofs is used to discretize the domain as shown in Figure 9b. For reference, the classical FEM scheme is used to solve the same problem with a highly refined conforming mesh ($h = 0.005$) with over 72,000 dofs.

Figure 10a compares the distribution of the σ_{22} stress component computed from the NIGFEM solution (left) with its reference FEM counterpart (right). As apparent there, the NIGFEM successfully predicts the stress field. Depicted in Figure 10b, the variation of the effective stress along the line $A - B$ confirms this observation. It should be noted that the displacement field experiences large gradients in the neighborhood of the material interfaces. To capture these large gradients in a conventional FEM analysis, adaptive mesh refinement techniques are usually adopted. Likewise, an IGA requires a refinement on the NURBS patches adjacent to the interface in these situations [20]. In order to avoid the global refinement of a NURBS patch, it has recently been suggested to replace the B-spline basis functions utilized in NURBS with their more generalized form, known as T-splines [41]. Similarly, the use of T-splines as enrichments in a generalized IGA framework has also been suggested [28]. Recent work on the Bezier extraction of T-splines has also facilitated the uniform treatment of NURBS and T-splines in IGA [42]. In comparison with these methods, the NIGFEM offers a more simple and practical approach to perform local mesh refinement using conventional NURBS (B-Spline) functions while successfully capturing the gradient field along the interface.

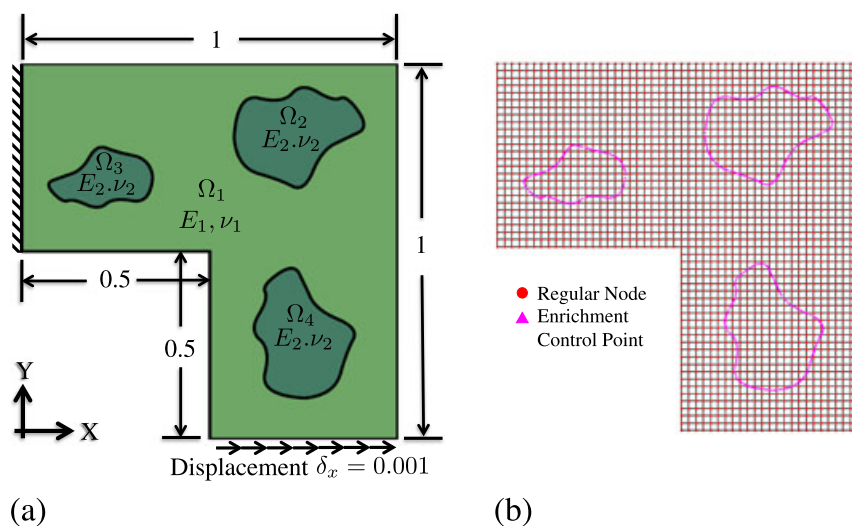
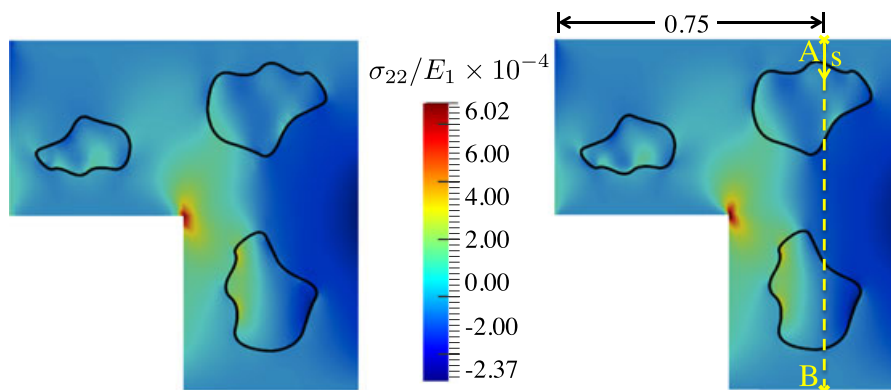
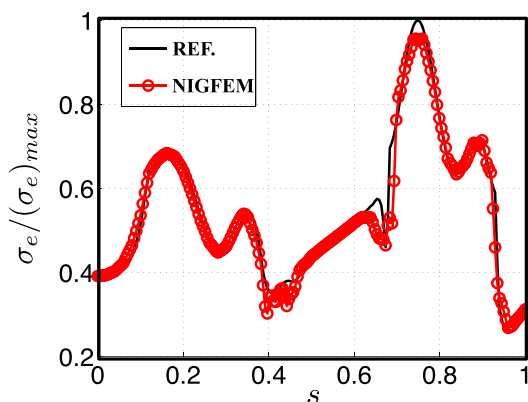


Figure 9. (a) Application problem with L-shaped domain containing three irregular inclusions. (b) Structured mesh adopted with the NIGFEM solver.



(a)



(b)

Figure 10. (a) Comparison of σ_{22} stress distribution obtained with the NIGFEM scheme (left) and reference FEM solution (right). (b) Distribution of normalized effective von Mises stress $\sigma_e/(\sigma_e)_{max}$ along line $A-B$.

5. CONCLUSIONS

The formulation and implementation of a NIGFEM for solving 2D planar elasticity problems have been presented. The NIGFEM utilizes NURBS to augment the finite element approximation space and minimize geometric errors associated with the discretization of a complex domain. The method presented in this manuscript shows a great potential in capturing discontinuous gradients along complex-shaped interfaces with relatively coarse non-conforming meshes. The use of NURBS in the enrichment of the finite element solution in the elements intersected by the material interfaces provides a natural and accurate way to capture the geometrical details of the internal boundaries. Two integration schemes have been presented and compared, showing the superior precision and lower computational cost of the SWM approach. The application problem has illustrated the ability of the method to simulate the structural response of a heterogeneous component with complex-shaped inclusions. The potential of the NIGFEM observed in this 2D study is likely to be especially attractive in a 3D setting, where the creation of conforming meshes is substantially more complex.

ACKNOWLEDGEMENTS

This work has been supported through a grant no. FA9550-12-1-0445 to the Center of Excellence on Integrated Materials Modeling (CEIMM) at Johns Hopkins University (partners JHU, UIUC, and UCSB) awarded by the AFOSR/RSL (Computational Mathematics Program, Manager Dr. F. Fahroo) and AFRL/RX (Monitors Dr. C. Woodward and T. Breitzman). Additional support was provided by Air Force Office of Scientific Research MURI (grant no. FA9550-09-1-0686).

REFERENCES

1. Melenk JM, Babuška I. The partition of unity finite element method: basic theory and applications. *Computer Methods in Applied Mechanics and Engineering* 1996; **139**(1–4):289–314.
2. Duarte CA, Babuška I, Oden JT. Generalized finite element methods for three-dimensional structural mechanics problems. *Computers & Structures* 2000; **77**(2):215–232.
3. Belytschko T, Gracie R, Ventura G. A review of extended/generalized finite element methods for material modeling. *Modelling and Simulation in Materials Science and Engineering* 2009; **17**(4):043001.
4. Fries TP, Belytschko T. The extended/generalized finite element method: an overview of the method and its applications. *International Journal for Numerical Methods in Engineering* 2010; **84**(3):253–304.
5. Babuška I, Melenk JM. The partition of unity method. *International Journal for Numerical Methods in Engineering* 1997; **40**(4):727–758.
6. Belytschko T, Black T. Elastic crack growth in finite elements with minimal remeshing. *International Journal for Numerical Methods in Engineering* 1999; **45**(5):601–620.
7. Moës N, Dolbow J, Belytschko T. A finite element method for crack growth without remeshing. *International Journal for Numerical Methods in Engineering* 1999; **46**(1):131–150.
8. Strouboulis T, Copps K, Babuška I. The generalized finite element method: an example of its implementation and illustration of its performance. *International Journal for Numerical Methods in Engineering* 2000; **47**(8):1401–1417.
9. Fries TP. A corrected XFEM approximation without problems in blending elements. *International Journal for Numerical Methods in Engineering* 2008; **75**(5):503–532.
10. Soghrati S, Aragón AM, Armando Duarte C, Geubelle PH. An interface-enriched generalized fem for problems with discontinuous gradient fields. *International Journal for Numerical Methods in Engineering* 2012; **89**(8):991–1008.
11. Sukumar N, Chopp DL, Moës N, Belytschko T. Modeling holes and inclusions by level sets in the extended finite element method. *Computer Methods in Applied Mechanics and Engineering* 2001; **190**(46–47):6183–6200.
12. Chessa J, Smolinski P, Belytschko T. The extended finite element method (XFEM) for solidification problems. *International Journal for Numerical Methods in Engineering* 2002; **53**(8):1959–1977.
13. Merle R, Dolbow J. Solving thermal and phase change problems with the extended finite element method. *Computational Mechanics* 2002; **28**(5):339–350.
14. Ji H, Chopp D, Dolbow JE. A hybrid extended finite element/level set method for modeling phase transformations. *International Journal for Numerical Methods in Engineering* 2002; **54**(8):1209–1233.
15. Cheng KW, Fries TP. Higher-order XFEM for curved strong and weak discontinuities. *International Journal for Numerical Methods in Engineering* 2010; **82**(5):564–590.
16. Haasemann G, Kästner M, Prüger S, Ulbricht V. Development of a quadratic finite element formulation based on the XFEM and NURBS. *International Journal for Numerical Methods in Engineering* 2011; **86**(4–5):598–617.
17. Benowitz BA, Waisman H. A spline-based enrichment function for arbitrary inclusions in extended finite element method with applications to finite deformations. *International Journal for Numerical Methods in Engineering* 2013; **95**(5):361–386.
18. Joulaian M, Düster A. Local enrichment of the finite cell method for problems with material interfaces. *Computational Mechanics* 2013; **52**(4):741–762.
19. Rogers DF. *An introduction to NURBS: with historical perspective* (1st edn), The Morgan Kaufmann Series in Computer Graphics. Morgan Kaufmann Publishers: San Francisco, 2000.
20. Hughes TJR, Cottrell JA, Bazilevs Y. Isogeometric analysis: CAD, finite elements, NURBS, exact geometry and mesh refinement. *Computer Methods in Applied Mechanics and Engineering* 2005; **194**(39–41):4135–4195.
21. Bazilevs Y, Beirao da Veiga L, Cottrell JA, Hughes TJR, Sangalli G. Isogeometric analysis: approximation, stability and error estimates for h-refined meshes. *Mathematical Models and Methods in Applied Sciences* 2006/07/01; **16**(07):1031–1090.
22. Bazilevs Y, Calo VM, Zhang Y, Hughes TJR. Isogeometric fluid–structure interaction analysis with applications to arterial blood flow. *Comput Mech* 2006; **38**(4–5):310–322.
23. Cottrell JA, Reali A, Bazilevs Y, Hughes TJR. Isogeometric analysis of structural vibrations. *Computer Methods in Applied Mechanics and Engineering* 2006; **195**(41–43):5257–5296.
24. Gómez H, Calo VM, Bazilevs Y, Hughes TJR. Isogeometric analysis of the Cahn–Hilliard phase-field model. *Computer Methods in Applied Mechanics and Engineering* 2008; **197**(49–50):4333–4352.
25. Verhoosel CV, Scott MA, Hughes TJR, de Borst R. An isogeometric analysis approach to gradient damage models. *International Journal for Numerical Methods in Engineering* 2011; **86**(1):115–134.
26. Benson DJ, Bazilevs Y, De Luycker E, Hsu MC, Scott M, Hughes TJR, Belytschko T. A generalized finite element formulation for arbitrary basis functions: from isogeometric analysis to XFEM. *International Journal for Numerical Methods in Engineering* 2010; **83**(6):765–785.
27. Sevilla R, Fernández-Méndez S, Huerta Antonio. NURBS-enhanced finite element method (NEFEM). *International Journal for Numerical Methods in Engineering* 2008; **76**(1):56–83.
28. Kim HJ, Seo YD, Youn SK. Isogeometric analysis for trimmed CAD surfaces. *Computer Methods in Applied Mechanics and Engineering* 2009; **198**(37–40):2982–2995.
29. Schmidt R, Wüchner R, Bletzinger KU. Isogeometric analysis of trimmed NURBS geometries. *Computer Methods in Applied Mechanics and Engineering* 2012; **241–244**(0):93–111.
30. Piegl LA, Tiller W. *The NURBS Book*. U.S. Government Printing Office, Springer: New York, 1997.

31. Hughes TJR, Reali A, Sangalli G. Efficient quadrature for NURBS-based isogeometric analysis. *Computer Methods in Applied Mechanics and Engineering* 2010; **199**(5–8):301–313.
32. Sevilla R, Fernández-Méndez S. Numerical integration over 2D NURBS-shaped domains with applications to NURBS-enhanced FEM. *Finite Elements in Analysis and Design* 2011; **47**(10):1209–1220.
33. Lipton S, Evans JA, Bazilevs Y, Elguedj T, Hughes TJR. Robustness of isogeometric structural discretizations under severe mesh distortion. *Computer Methods in Applied Mechanics and Engineering* 2010; **199**(5–8):357–373.
34. Cohen E, Martin T, Kirby RM, Lyche T, Riesenfeld RF. Analysis-aware modeling: understanding quality considerations in modeling for isogeometric analysis. *Computer Methods in Applied Mechanics and Engineering* 2010; **199**(5–8):334–356.
35. Strouboulis T, Babuška I, Coppers K. The design and analysis of the generalized finite element method. *Computer Methods in Applied Mechanics and Engineering* 2000; **181**(1–3):43–69.
36. Park K, Pereira JP, Duarte CA, Paulino GH. Integration of singular enrichment functions in the generalized/extended finite element method for three-dimensional problems. *International Journal for Numerical Methods in Engineering* 2009; **78**(10):1220–1257.
37. Mousavi SE, Grinspun E, Sukumar N. Higher-order extended finite elements with harmonic enrichment functions for complex crack problems. *International Journal for Numerical Methods in Engineering* 2011; **86**(4–5):560–574.
38. Daux C, Moës N, Dolbow J, Sukumar N, Belytschko T. Arbitrary branched and intersecting cracks with the extended finite element method. *International Journal for Numerical Methods in Engineering* 2000; **48**(12):1741–1760.
39. Van Miegroet L, Duysinx P. Stress concentration minimization of 2D fillets using X-FEM and level set description. *Structural and Multidisciplinary Optimization* 2007; **33**(4–5):425–438.
40. Srinivasan KR, Matouš K, Geubelle PH. Generalized finite element method for modeling nearly incompressible bimaterial hyperelastic solids. *Computer Methods in Applied Mechanics and Engineering* 2008; **197**(51–52):4882–4893.
41. Bazilevs Y, Calo VM, Cottrell JA, Evans JA, Hughes TJR, Lipton S, Scott MA, Sederberg TW. Isogeometric analysis using T-splines. *Computer Methods in Applied Mechanics and Engineering* 2010; **199**(5–8).
42. Scott MA, Borden MJ, Verhoosel CV, Sederberg TW, Hughes TJR. Isogeometric finite element data structures based on Bézier extraction of T-splines. *International Journal for Numerical Methods in Engineering* 2011; **88**(2):126–156.